

# Interplay of dilution and magnetic field in the nearest-neighbor spin-ice model on the pyrochlore lattice

Alexey Peretyatko<sup>1,\*</sup>, Konstantin Nefedev<sup>1,2,†</sup> and Yutaka Okabe<sup>3‡</sup>

<sup>1</sup>*School of Natural Sciences, Far Eastern Federal University,  
Vladivostok, Russian Federation*

<sup>2</sup>*Institute of Applied Mathematics,  
Far Eastern Branch, Russian Academy of Science,  
Vladivostok, Russian Federation*

<sup>3</sup>*Department of Physics, Tokyo Metropolitan University,  
Hachioji, Tokyo 192-0397, Japan*

(Dated: September 9, 2018)

We study the magnetic field effects on the diluted spin-ice materials using the replica-exchange Monte Carlo simulation. We observe *five* plateaus in the magnetization curve of the diluted nearest-neighbor spin-ice model on the pyrochlore lattice when a magnetic field is applied in the [111] direction. This is in contrast to the case of the pure model with two plateaus. The origin of *five* plateaus is investigated from the spin configuration of two corner-sharing tetrahedra in the case of the diluted model.

PACS numbers: 75.40.Mg, 75.50.Lk, 64.60.De

Spin-ice materials have captured a lot of attention [1–3], and their exotic physics is a current topic of geometrically frustrated magnets. Prototype materials are pyrochlores  $\text{Dy}_2\text{Ti}_2\text{O}_7$  and  $\text{Ho}_2\text{Ti}_2\text{O}_7$ . Magnetic field effects, especially the existence of plateaus, have been studied theoretically [4–6] and experimentally [7–11].

In spin-ice materials, magnetic ions ( $\text{Dy}^{3+}$  or  $\text{Ho}^{3+}$ ) occupy the pyrochlore lattice of corner-sharing tetrahedra, and the local crystal field environment causes magnetic moments to point along the lines connecting the centers of the two tetrahedra at low temperatures. In the low-temperature spin-ice state, magnetic moments are highly constrained locally and obey the so-called “ice rules”: two spins point in and two spins point out of each tetrahedron of the pyrochlore lattice. This 2-in 2-out spin configuration is equivalent to the situation for hydrogen atoms in water ice [12].

The dilution effect on frustration was studied by Ke *et al.* [13] for spin-ice materials. Magnetic ions Dy or Ho are replaced by nonmagnetic Y ions. Nonmonotonic zero-point entropy as a function of the dilute concentration was observed experimentally, and further studies on the dilution effects have been reported [14–16].

In this communication, we study the diluted nearest-neighbor (NN) antiferromagnetic (AFM) Ising model on the pyrochlore lattice under a magnetic field in the [111] direction. We treat the NN interaction as a theoretical model; a more complicated model, such as the dipolar model, may be required to make connections to actual materials. For the simulation method, we use the replica-exchange Monte Carlo method [17] to avoid the trap at

local-minimum configurations.

We are concerned with the Hamiltonian, which is given in Eq. (2.2) of Ref. [6];

$$H = J \sum_{\langle i,j \rangle} \sigma_i \sigma_j - \sum_i \mathbf{h} \cdot \mathbf{d}_{\kappa(i)} \sigma_i, \quad (1)$$

where  $J(>0)$  is the effective antiferromagnetic coupling,  $\sigma_i$  are the Ising pseudospins ( $\sigma_i = \pm 1$ ), and  $\langle i,j \rangle$  stands for the NN pairs. The unit vectors  $\mathbf{d}_{\kappa(i)}$  are the local easy axes of the pyrochlore lattice, and explicitly described as  $\mathbf{d}_{\kappa(i)} = \{\mathbf{d}_0, \mathbf{d}_1, \mathbf{d}_2, \mathbf{d}_3\}$ , where  $\mathbf{d}_0 = (1, 1, 1)/\sqrt{3}$ ,  $\mathbf{d}_1 = (1, -1, -1)/\sqrt{3}$ ,  $\mathbf{d}_2 = (-1, 1, -1)/\sqrt{3}$ , and  $\mathbf{d}_3 = (-1, -1, 1)/\sqrt{3}$ . We consider the case when the magnetic field  $\mathbf{h}$  is along the [111] direction; that is,  $\mathbf{h} = h\mathbf{d}_0$ . Then,  $\mathbf{h} \cdot \mathbf{d}_{\kappa(i)}$  becomes  $h$  for apical spins where  $\mathbf{d}_{\kappa(i)} = \mathbf{d}_0$ , but  $-(1/3)h$  for other spins. The magnetization  $M$  along the [111] direction is calculated through the relation

$$M = \sum_i \mathbf{d}_0 \cdot \mathbf{d}_{\kappa(i)} \sigma_i. \quad (2)$$

For convenience, the illustration of the pyrochlore lattice, which is a three-dimensional network of corner-sharing tetrahedra, is given in Fig. 1, where the apical spins,  $\mathbf{d}_{\kappa(i)} = \mathbf{d}_0$ , are shown in red, whereas other spins are in blue.

In the case of the site dilution of spins, the Hamiltonian becomes

$$H = J \sum_{\langle i,j \rangle} c_i c_j \sigma_i \sigma_j - \sum_i \mathbf{h} \cdot \mathbf{d}_{\kappa(i)} c_i \sigma_i. \quad (3)$$

Here  $c_i$  are the quenched variables ( $c_i = 1$  or  $0$ ), and the concentration of vacancies is denoted by  $x$ .

The Monte Carlo simulation has become a standard method to study many-body problems in physics. How-

\*Electronic address: peretyatko.aa@dvfu.ru

†Electronic address: nefedev.kv@dvfu.ru

‡Electronic address: okabe@phys.se.tmu.ac.jp

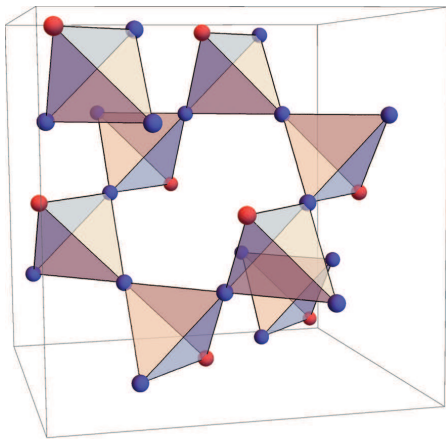


FIG. 1: (Color online.) The illustration of the pyrochlore lattice, which is a three-dimensional network of corner-sharing tetrahedra. The apical spins,  $\mathbf{d}_{\kappa(i)} = \mathbf{d}_0$ , are shown in red, whereas other spins are in blue.

ever, we sometimes suffer from the problem of slow dynamics. One attempt to solve the problem of slow dynamics is the extended ensemble method. The replica-exchange Monte Carlo method or parallel tempering [17, 18] is an example. The replica-exchange method has been successfully applied to various systems, for example, in the problem of spin glasses [19]. The idea of replica-exchange can be combined with the molecular dynamics simulation. Using this combined method, the protein-folding problem was studied [20].

Let us consider two replicas of a system. If the inverse temperature of the replica 1 is  $\beta_1$  and that of the replica 2 is  $\beta_2$ , the Boltzmann weight of the composite system is  $\exp[-(\beta_1 E_1 + \beta_2 E_2)]$ , where  $E_1$  and  $E_2$  are the energy of each system. We try to exchange two replica systems, or exchange two inverse temperatures. If we make this exchange trial using the transition probability based on the relative Boltzmann weight,

$$\begin{aligned} & \exp[-(\beta_1 E_2 + \beta_2 E_1) + (\beta_1 E_1 + \beta_2 E_2)] \\ & = \exp[(\beta_1 - \beta_2)(E_1 - E_2)], \end{aligned}$$

the Boltzmann distribution of the composite system is guaranteed. In the actual calculation, we may use many replicas. We note that replicas are not necessarily for several temperatures; we can also use replicas for several magnetic fields. In the present simulation, we treat 546 systems of 91 magnetic fields and 6 temperatures simultaneously. To escape from the local-minimum trap problem, the loop algorithm is sometimes employed [6]. Here, we use the replica-exchange method for both temperature and magnetic field based on the single spin flip. The convergence is good enough even for low temperatures such as  $T/J = 0.05$ .

For the simulation of the AFM Ising model on the pyrochlore lattice, we used a 16-site cubic unit cell of the pyrochlore lattice, and systems with  $L \times L \times L$  unit cells

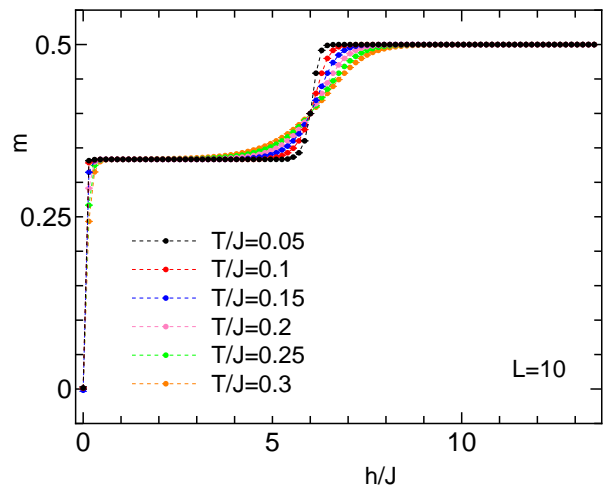


FIG. 2: (Color online) The magnetization curve for the AFM Ising model on the pyrochlore lattice. The magnetic field is applied in the [111] direction. The system size is  $L = 10$  ( $N = 16000$ ), and the temperature is  $T/J = 0.05, 0.1, 0.15, 0.2, 0.25,$  and  $0.3$ .

with periodic boundary conditions were treated. We performed simulations for the system sizes of  $L = 6, 8,$  and  $10$ ; the numbers of sites were  $N = 3456, 8192,$  and  $16000$ , respectively. As for the dilute concentration  $x$ , we treated  $x = 0.0$  (pure),  $0.2, 0.4, 0.6,$  and  $0.8$ . We discarded the first 5,000 Monte Carlo Steps (MCSs) to avoid the effects of initial configurations, and the next 50,000 MCSs were used for the measurement. We took an average over 20 samples for each size and each  $x$  to estimate the statistical errors.

We start with showing the results of the pure (non-diluted) model ( $x = 0.0$ ). In Fig. 2 the magnetization  $m = M/N$  is plotted as a function of the applied field  $h$ . The system size is  $L = 10$  ( $N = 16000$ ). We plot the data for the temperatures  $T/J = 0.05, 0.1, 0.15, 0.2, 0.25,$  and  $0.3$ . The average was taken over 20 samples with different random-number sequences. The statistical errors are within the size of the marks. The size  $L = 10$  is large enough; the size dependence is small. We confirmed the two plateaus in the magnetization curve; in the first of which the ground-state entropy is reduced but still remains extensive [5, 6]. The height of the plateau jumps from  $m = 1/3$  to  $m = 1/2$  at  $h/J = 6$ , and the jump becomes smoother when raising the temperature. The pyrochlore lattice can be regarded as alternating kagome and triangular layers, and the [111] magnetic field effectively decouples these layers. We can see in Fig. 1 that blue spins form the kagome lattice. The states with  $m = 1/3$  still have macroscopic degeneracy, and sometimes called as "kagome-ice" states [8, 9]. The magnetization of  $m = 1/2$  is the maximum magnetization for this problem.

The proportion of the types of spin configurations in the tetrahedron for the AFM Ising model on the py-

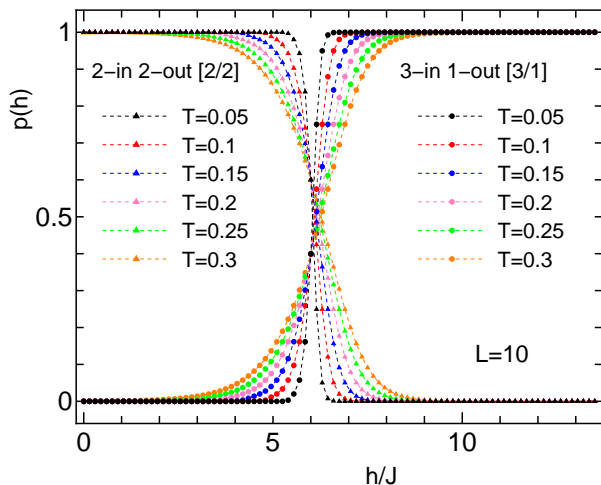


FIG. 3: (Color online) The proportion of the types of spin configurations in the tetrahedron for the AFM Ising model on the pyrochlore lattice under the magnetic field. The magnetic field is applied in the [111] direction. The system size is  $L = 10$  ( $N = 16000$ ), and the temperature is  $T/J = 0.05, 0.1, 0.15, 0.2, 0.25,$  and  $0.3$ .

pyrochlore lattice under the magnetic field in the [111] direction is plotted in Fig. 3. There are 8000 tetrahedra for  $L = 10$ , and the proportion of the types of spin configurations was measured for 50,000 MCSs. An average over 20 independent samples to estimate the error bars. The type of spin configurations is classified by the numbers of up (+) spins and those of down (-) spins in the tetrahedron. The up spin points "out" in one tetrahedron, but it points "in" in the adjacent tetrahedron. Here, we use the notation "out" for up spin and the notation "in" for down spin to express a spin configuration. We clearly see the change from the 2-in 2-out configuration to the 3-in 1-out configuration at  $h/J = 6$ . The change becomes smoother when the temperature is raised.

Next, we consider the results of diluted systems. We plot the magnetization curve for the diluted AFM Ising model on the pyrochlore lattice in Fig. 4. The system size is  $L = 10$  ( $N = 16000$ ), and the temperature is  $T/J = 0.05$ . The dilute concentration ( $x$ ) is 0.0, 0.2, 0.4, 0.6, and 0.8. The average was taken over 20 random samples. The error bars are shown in the figure, but they are within the size of marks. The random average over 20 samples yields small statistical errors for large enough system size of  $L = 10$  ( $N = 16000$ ).

We observe five plateaus in the magnetization curve of diluted systems; for  $h/J < 3$ ,  $3 < h/J < 6$ ,  $6 < h/J < 9$ ,  $9 < h/J < 12$ , and  $h/J > 12$ . This is in contrast to the pure case where only two plateaus are separated at  $h/J = 6$ . We plot the results of  $T/J = 0.05$ ; if the temperature is raised, the magnetization step becomes smoother. The saturated value of the magnetization  $m$  is  $(1/2) * (1 - x)$ .

In the case of the pure model, the spin configuration of

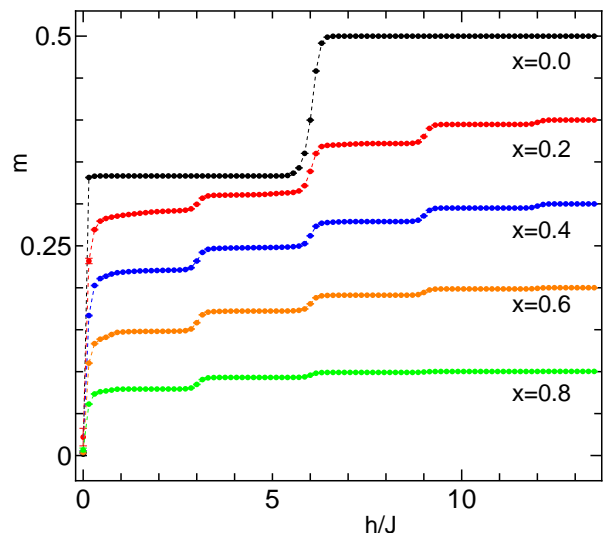


FIG. 4: (Color online) The magnetization curve for the diluted AFM Ising model on the pyrochlore lattice. The system size is  $L = 10$  ( $N = 16000$ ), and the temperature is  $T/J = 0.05$ . The dilute concentration ( $x$ ) is 0.0, 0.2, 0.4, 0.6, and 0.8.

the tetrahedron changes from the 2-in 2-out configuration to the 3-in 1-out configuration when the magnetic field is applied in the [111] direction. On the contrary, the spin configuration becomes more complex for diluted systems. The situation becomes different if an apical spin is deleted or another spin is deleted. The magnetic field dependence of the spin configuration is plotted in Fig. 5. The system size is  $L = 10$  ( $N = 16000$ ), and the temperature is  $T/J = 0.05$ . The dilute concentration ( $x$ ) is 0.2 and 0.4. There are 8000 tetrahedra for  $L = 10$ , and the number of spins in the tetrahedron,  $n$ , becomes 4, 3, 2, 1, or 0 for diluted systems.

The top panel of Fig. 5 is the plot for the spin number  $n = 4$ . The number of spins,  $n$ , is 4 for about 41% of tetrahedra in the case of  $x = 0.2$ , and about 13% in the case of  $x = 0.4$ . The change from the 2-in 2-out configuration, [2/2], to the 3-in 1-out configuration, [3/1], is observed at  $h/J = 6$  as in the pure case. However, the proportions of [2/2] and [3/1] also change at  $h/J = 3$  and at  $h/J = 9$ .

The middle panel of Fig. 5 is the plot for the spin number  $n = 3$ . There are two possibilities that the deleted spin is an apical spin and that is another spin. When the apical spin is not deleted, the partial change from the 1-in 2-out configuration, [1/2+], to the 2-in 1-out configuration, [2/1+], is observed. When the apical spin is deleted, the change from the 2-in 1-out configuration, [2/1-], to the 3-in 0-out configuration, [3/0-], is observed with two steps at  $h/J = 9$  and at  $h/J = 12$ . For the low- $h$  region, the 1-in 2-out configuration, [1/2-], remains. We use the notations "+" and "-" to specify the configuration whether the apical spin is deleted (" - ") or not deleted

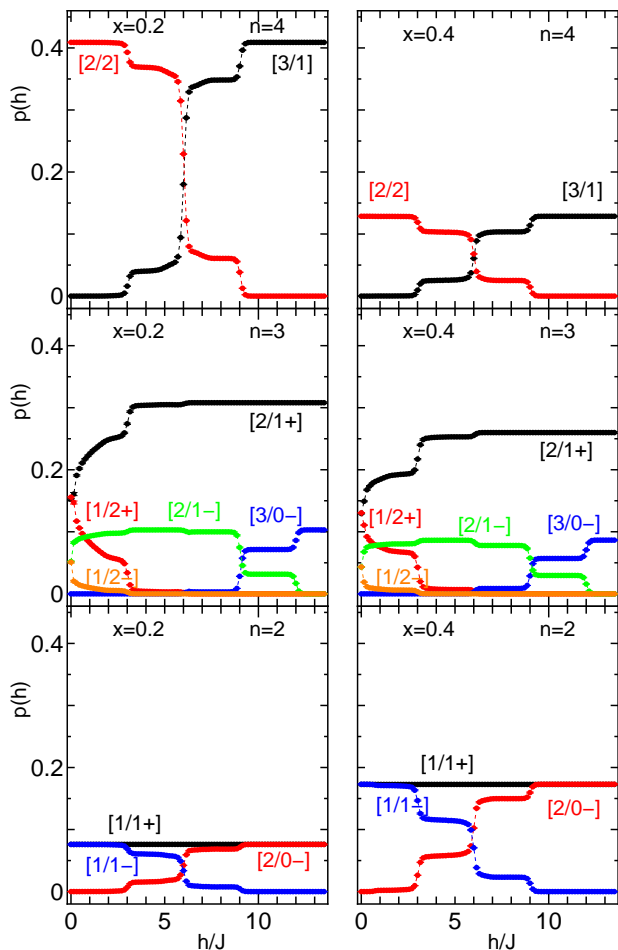


FIG. 5: (Color online) The proportion of the types of spin configurations in the tetrahedron for the diluted AFM Ising model on the pyrochlore lattice under the magnetic field in the [111] direction. The system size is  $L = 10$  ( $N = 16000$ ), and the temperature is  $T/J = 0.05$ . The dilute concentration ( $x$ ) is 0.2 (left) and 0.4 (right). The number of spins  $n$  in the tetrahedron is 4, 3, and 2 for the top, middle, and bottom panel, respectively.

("+"). Thus,  $[2/1+]$ , for example, stands for the 2-in 1-out configuration where there are three spins including the apical spin in the tetrahedron.

The bottom panel of Fig. 5 is the plot for the spin number  $n = 2$ . Two spins are deleted from the tetrahedron. If the apical spin is not deleted, the 1-in 1-out configuration,  $[1/1+]$ , is stable. When one apical spin is deleted, the change from the 1-in 1-out configuration,  $[1/1-]$ , to the 2-in 0-out configuration,  $[2/0-]$ , at  $h/J = 6$  is observed. The variation in the proportions is observed at  $h/J = 3$  and  $h/J = 9$ .

We showed the data for  $x = 0.2$  and 0.4, and we see the dilute concentration ( $x$ ) dependence. The situation is essentially the same, although the proportion of smaller  $n$  in the tetrahedron increases when  $x$  becomes larger. For

TABLE I: The local energy of the spin configuration in the tetrahedron for the spin numbers  $n = 4, 3$ , and 2. When the magnetic field is applied in the [111] direction, the apical spin is fixed as "out".

config.	$n$ spins	apical ("out")	"in"	"out"	energy
$[3/1]$	4	1	3	0	$-6(h/6)$
$[2/2]$		1	2	1	$-2J - 4(h/6)$
$[2/1+]$	3	1	2	0	$-J - 5(h/6)$
$[1/2+]$		1	1	1	$-J - 3(h/6)$
$[3/0-]$		0	3	0	$3J - 3(h/6)$
$[2/1-]$		0	2	1	$-J - (h/6)$
$[1/2-]$		0	1	2	$-J + (h/6)$
$[1/1+]$	2	1	1	0	$-J - 4(h/6)$
$[2/0-]$		0	2	0	$J - (h/6)$
$[1/1-]$		0	1	1	$-J$

strong dilution, such as  $x = 0.8$ , there appear many free spins, which do not create a magnetization step; the magnetization jump becomes smaller for larger  $x$ . Even the proportion of tetrahedra with no spins ( $n = 0$ ) increases, which do not have magnetization.

Now, we elucidate the origin of the five plateaus in the magnetization curve. We investigate the local energy of the spin configuration of tetrahedron for spin numbers  $n = 4, 3$ , and 2, which is tabulated in Table I. The apical spin is fixed as "out" when the magnetic field is applied in the [111] direction. The sum of "in" and "out" spins of other spins is  $n - 1$  when the apical spin is not deleted, whereas that is  $n$  when the apical spin is deleted. The local energy for each configuration is given in the last column. We note that the Zeeman energy term is shared by two tetrahedra.

We consider the energy of two corner-sharing tetrahedra. In Fig. 6, the flip process is schematically illustrated. The apical spins are denoted by the long red arrow, whereas other spins are denoted by the short blue arrow. We note that  $\mathbf{d}_0 \cdot \mathbf{d}_{\kappa(i)} = 1$  for the apical spin, whereas that is  $-1/3$  for other spins. The deleted spins are denoted by the empty circle. The case when the two tetrahedra are  $n = 4$  is shown in (i). When the corner-sharing spin is turned from "out" to "in", the configuration is changed from  $([2/2]+[2/2])$  to  $([3/1]+[3/1])$ . From Table I the crossover magnetic field is calculated by

$$2(-2J - 4(h/6)) = 2(-6(h/6)).$$

Then, we get  $h_c/J = 6$ . The cases when the two tetrahedra are  $n = 4$  and  $n = 3$  are shown in (ii) and (iii). When the corner-sharing spin is turned from "out" to "in", the configuration is changed from  $([2/2]+[1/2+])$  to  $([3/1]+[2/1+])$  in (ii). From Table I the crossover magnetic field is calculated by

$$\begin{aligned} &(-2J - 4(h/6)) + (-J - 3(h/6)) \\ &= (-6(h/6)) + (-J - 5(h/6)). \end{aligned}$$

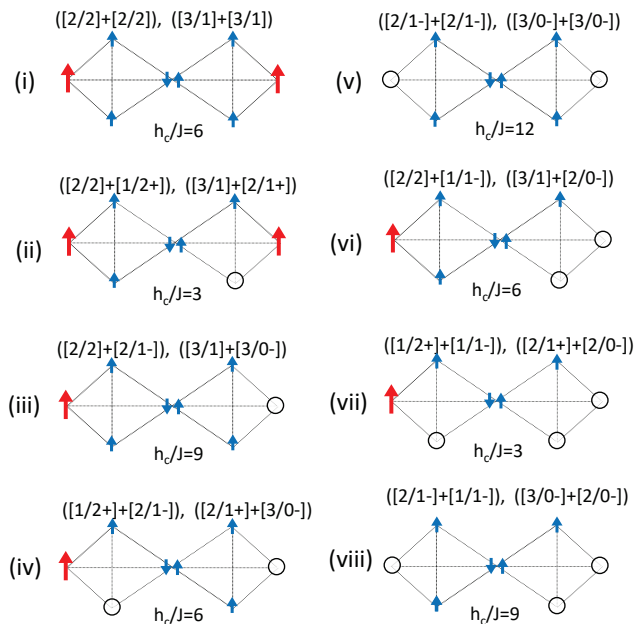


FIG. 6: (Color online) The schematic illustration of spin flip for corner-sharing tetrahedra. The apical spins are denoted by the long red arrow, whereas other spins are denoted by the short blue arrow. The deleted spins are denoted by the empty circle. The cases that two tetrahedra are  $n = 4, 3, 2$  are shown in (i) ~ (viii). The crossover values  $h_c$  are given there.

Then, we get  $h_c/J = 3$ . A similar consideration yields  $h_c/J = 9$  for the change from  $([2/2]+[2/1-])$  to  $([3/1]+[3/0-])$  in (iii) from the relation

$$\begin{aligned} &(-2J - 4(h/6)) + (-J - (h/6)) \\ &= (-6(h/6)) + (3J - 3(h/6)). \end{aligned}$$

The cases when both are  $n = 3$  are shown in (iv) and (v). The case that two tetrahedra are  $n = 4$  and  $n = 2$  is shown in (vi). The cases when they are  $n = 3$  and  $n = 2$  are shown in (vii) and (viii). The crossover values  $h_c$  can be obtained in the same way as before, and they are given in Fig. 6.

This investigation clearly accounts for the change in the configurations given in Fig. 5, which leads to the elucidation of the *five* magnetization plateaus shown in

Fig. 4.

To summarize, we studied the magnetic field effects on diluted spin-ice materials using the replica-exchange Monte Carlo simulation. We observed *five* plateaus in the magnetization curve of the diluted NN spin-ice model on the pyrochlore lattice when a magnetic field was applied in the [111] direction. This is in contrast to the case of the pure model with two plateaus. The origin of the *five* plateaus was investigated from the spin configuration of two corner-sharing tetrahedra in the case of the diluted model.

As for the actual material, the magnetization step was observed around 0.9 Tesla for  $\text{Dy}_2\text{Ti}_2\text{O}_7$ [9, 22]. In the diluted system, more steps could be observed at the half magnetic field ( $h/J = 3$ ) of the pure system ( $h/J = 6$ ) and at the one-and-a-half magnetic field ( $h/J = 9$ ). These two new steps are rather easy to be observed because these steps appear when a single spin is deleted from two corner-sharing tetrahedra (See (ii) and (iii) in Fig. 6). On the other hand, the step at  $h/J = 12$  is smaller because this happens only when the two spins in the adjacent tetrahedra are deleted (See (v) in Fig. 6), although the change of spin configuration is observed at  $h/J = 12$  as in the middle panel of Fig. 5 even for large  $x$ . We treated the diluted NN spin-ice model. The long-range dipolar interaction may have some effects, although the important point is the interplay of dilution and magnetic field for frustrated systems. The competition between the pair interaction term and the Zeeman term becomes complex when spins are deleted. Experimental researches are awaited.

Antiferromagnetic spin systems on the pyrochlore lattice provide a rich variety of physics of frustrated systems. In the present communication we discussed the interplay of dilution and magnetic field. The relevance to the magnetic monopoles picture [21, 22] will be an interesting problem. The effects of magnetic fields in other directions considering the Kasteleyn transition [23] is left to a future work.

We thank Vitalii Kapitan, Yuriy Shevchenko, and Konstantin Soldatov for valuable discussions. The computer cluster of Far Eastern Federal University was used for computation. This work was supported by a Grant-in-Aid for Scientific Research from the Japan Society for the Promotion of Science, Grant Numbers JP25400406, JP16K05480.

[1] M. J. Harris, S. T. Bramwell, D. F. McMorrow, T. Zeiske, and K.W. Godfrey, Phys. Rev. Lett. **79**, 2554 (1997).  
[2] A. P. Ramirez, A. Hayashi, R. J. Cava, R. Siddharthan, and B. S. Shastry, Nature (London) **399**, 333 (1999).  
[3] S. T. Bramwell and M. J. P. Gingras, Science **294**, 1495 (2001).  
[4] M. J. Harris, S. T. Bramwell, P. C. W. Holdsworth, and J. D. M. Champion, Phys. Rev. Lett. **81**, 4496 (1998).

[5] R. Moessner and S. L. Sondhi, Phys. Rev. B **68**, 064411 (2003).  
[6] S. V. Isakov, K. S. Raman, R. Moessner, and S. L. Sondhi, Phys. Rev. B **70**, 104418 (2004).  
[7] K. Matsuhira, Z. Hiroi, T. Tayama, S. Takagi, and T. Sakakibara, J. Phys.: Condens. Matter **14**, L559 (2002).  
[8] Z. Hiroi, K. Matsuhira, S. Takagi, T. Tayama, and T. Sakakibara, J. Phys. Soc. Jpn. **72**, 411 (2003).

- [9] T. Sakakibara, T. Tayama, Z. Hiroi, K. Matsuhira, and S. Takagi, *Phys. Rev. Lett.* **90**, 207205 (2003).
- [10] R. Higashinaka, H. Fukazawa, and Y. Maeno, *Phys. Rev. B* **68**, 014415 (2003).
- [11] H. Fukazawa, R. G. Melko, R. Higashinaka, Y. Maeno, and M. J. P. Gingras, *Phys. Rev. B* **65**, 054410 (2002).
- [12] L. Pauling, *J. Am. Chem. Soc.* **57**, 2680 (1935).
- [13] X. Ke, R. S. Freitas, B. G. Ueland, G. C. Lau, M. L. Dahlberg, R. J. Cava, R. Moessner, and P. Schiffer, *Phys. Rev. Lett.* **99**, 137203 (2007).
- [14] T. Lin, X. Ke, M. Thesberg, P. Schiffer, R. G. Melko, and M. J. P. Gingras, *Phys. Rev. B* **90**, 214433 (2014).
- [15] S. Scharffe, O. Breunig, V. Cho, P. Laschitzky, M. Vallador, J. F. Welter, and T. Lorenz, *Phys. Rev. B* **92**, 180405(R) (2015).
- [16] Y. Shevchenko, K. Nefedev, and Y. Okabe, unpublished.
- [17] K. Hukushima and K. Nemoto, *J. Phys. Soc. Jpn.* **65**, 1604 (1996).
- [18] E. Marinari, Optimized Monte Carlo methods, in *Advances in Computer Simulation*, edited by J. Kertész and I. Kondor (Springer-Verlag, 1998), p. 50.
- [19] L. W. Lee and A. P. Young, *Phys. Rev. Lett.* **90**, 227203 (2003).
- [20] Y. Sugita and Y. Okamoto, *Chem. Phys. Lett.* **314**, 141 (1999).
- [21] C. Castelnovo, R. Moessner, and S. L. Sondhi, *Nature* **451**, 42 (2008).
- [22] H. Kadowaki, N. Doi, Y. Aoki, and Y. Tabata, *J. Phys. Soc. Jpn.* **78**, 103706 (2009).
- [23] P.W. Kasteleyn, *J. Math. Phys.* **4**, 287 (1963).